Optics Communications 457 (2020) 124716

Contents lists available at ScienceDirect

Optics Communications

journal homepage: www.elsevier.com/locate/optcom

Effect of the changes in refractive index of air on grating diffraction wavefront

Xiaotao Mi *, Shanwen Zhang, Xiangdong Qi, Haili Yu, Hongzhu Yu, Yu Lin, Xuefeng Yao, Sibo Jiang, Jingxuan Zhou

Grating Technology Laboratory, Changchun Institute of Optics and Fine Mechanics and Physics, Chinese Academy of Sciences, Changchun, Jilin 130033, China

ARTICLE INFO

Keywords:
Gratings
The refractive index of air
Grating diffraction wavefront error

ABSTRACT

Reduction of groove errors on the grating wavefront caused by the refractive index of air is a critical issue in ruling grating fabrication when using an interferometer to provide position feedback. We establish a mathematical model of the relationship between the grating wavefront and the refractive index of air. We then introduce two methods to measure the air's refractive index, analyze the effects of temperature, pressure and humidity on the grating wavefront, and use the advantages of the two methods to obtain the groove error compensation value. Comparative ruling experiments prove that grating wavefront quality is significantly improved after compensation of the groove errors caused by the refractive index of air.

1. Introduction

The excellent functions of gratings, including dispersion, polarization and phase matching, have led to strong demand for these elements, with particularly high demand for high-quality, large-sized gratings in fields ranging from spectral analysis [1,2] to lasers [3,4], optical communications [5,6] and pulse compressors [7,8]. The interference method and mechanical ruling method are the main methods for fabricating master gratings. The interference methods include the laser beam interferometry using large size writing beams, which has been adopted to fabricate multilayer dielectric reflection grating with a diameter of up to 1 m by Lawrence Livermore National Laboratory (LLNL) [9], and the scanning beam interferometry using two small writing beams interfering on the substrate, which has been adopted to fabricate a 910 mm × 420 mm grating by Plymouth Grating Laboratory (PGL) [10]. The mechanical ruling method is the most important way to produce gratings that have deep grooves and strict shapes, such as echelle gratings and infrared laser gratings [11,12].

Ruling engines are used to fabricate the master gratings, and ruling engine development has been performed for more than a century, but the pursuit of higher precision ruling engines has never stopped [13–15]. The early grating ruling engines, and most of the later engines, were operated under open loop control conditions [16,17]. The accuracy of these engines is dependent on the mechanical accuracy of the important components and the engine assembly accuracy. In 1915, Michelson at the University of Chicago proposed control of the groove position using an interferometer. The laser interferometer, with its very high resolution, noncontact sensing capability, high stability, and high update rate, is the first choice for feedback equipment in the position servo loop of closed-loop-controlled ruling engines. In 1955, Harrison and Stroke put Michelson's suggestion of a servo system controlled by an interferometer into practice, and the ruling engine thus entered the era of closed-loop control; the grating groove positions were then determined based on the wavelength of the light and the accuracy and quality of the ruled grating improved significantly [18].

The variation in the refractive index of air due to the effects of temperature, pressure and humidity will cause wavelength variations, which in turn will affect the quality of gratings. For the grating fabricated by the interference method, the wavelength variations of the interference beam will cause changes in the grating groove density. For the scanning beam interference method using two small writing beams and mechanical ruling method, the laser interferometers are required as measurement and feedback components for high-precision stages, so the wavelength variations of the measuring beam will cause groove position errors. Therefore, the above methods for fabricating the gratings all require strict control of the change in refractive index of air.

Internationally, well-known closed-loop controlled ruling engines include the MIT-C engine, which is currently the largest ruling engine in the world and is able to rule blanks with dimensions of up to 450 mm × 650 mm × 125 mm [19], and the Hitachi-4 engine, which has ruled gratings with density of 10 000 grooves/mm [20]. In the MIT-C ruling engine system, the temperature variation of the ruling room is controlled to be better than ±0.005 °C, and pressure corrections are introduced automatically using a simple electrical analog computer [19]. The main part of the Hitachi-4 ruling engine is installed

* Corresponding author.
E-mail address: mixiaotao_ciomp@126.com (X. Mi).

https://doi.org/10.1016/j.optcom.2019.124716
Received 17 July 2019; Received in revised form 29 September 2019; Accepted 6 October 2019
Available online 10 October 2019

in a room with temperature stability of ±0.01 °C [20]; a wavelength compensation interferometer is used to measure any changes in the atmospheric conditions that affect the laser light wavelength, and the groove error caused by changes in the refractive index of air is then corrected in real time. However, there are no relevant publications in the literature that describe the effects of changes in the refractive index of air on the gratings.

In this work, we present a systematic study of the relationship between changes in the refractive index of air and the resulting grating diffraction wavefront error with a focus on improving the grating diffraction wavefront quality. We derive a mathematical model of the relationship between the grating wavefront and the refractive index of air. We then introduce two methods to measure the refractive index of the air, use the Edlen equation to analyze the effects of temperature, pressure and humidity on the grating wavefront, and we then make full use of the advantages of the two measurement methods to obtain a compensation value for the groove error. Finally, we prove experimentally that correction for changes in the refractive index of air can improve the grating diffraction wavefront significantly.

2. Mathematical model of changes in the refractive index of air and the grating diffraction wavefront error

The accuracy of ruling engine operation and surface errors on the grating blank are the two main factors that affect the grating groove position error. The grating ruling engines use laser interferometers as feedback elements and the groove positions are determined relative to the laser wavelength. Changes in the refractive index of air will affect the laser light's wavelength, which in turn affects the groove position errors and the grating performance. The relationship between the laser light wavelength at any time and the laser light wavelength under vacuum conditions can be written as:

$$n_c \times \lambda_c = n_t \times \lambda_t \tag{1}$$

where n_c is the vacuum refractive index, λ_c is the laser light wavelength under vacuum conditions, n_t is the refractive index of the air at time t, and λ_t is the laser light wavelength when the refractive index is n_t.

According to the displacement measurement principle of the laser interferometer, the measured displacement can be given by [21]

$$l = \frac{\lambda}{4}\int_0^t \Delta f \cdot dt = N\frac{\lambda}{4} \times \frac{1}{1024} \tag{2}$$

where λ is the laser light wavelength and N is the pulse count value.

We use the laser light wavelength under vacuum conditions as the reference wavelength. From Eqs. (1) and (2), the groove position error caused by the refractive index n_t at any time t can be calculated as follows:

$$\Delta l_t = l_c - l_t = (n_t - n_c) \cdot l_t \tag{3}$$

where Δl_t is the groove position error caused by the refractive index of air n_t, and l_t is the displacement measured using the laser interferometer when the refractive index of air is n_t.

The slow and irregular nature of the change in the refractive index of air means that it will mainly affect the diffraction wavefront of the grating. To simplify the analysis, we make the following two assumptions: (1) the plane of the grating blank is flat and thus does not affect grating performance; (2) the distance from the point on the metal film to the ideal ruling plane before the grating is ruled is the same as the distance from the corresponding point in the actual groove shape to the ideal groove shape after the grating is ruled. Based on the assumptions and analysis above, we ignore the detailed groove shape of the grating for simplicity, and the grating groove errors will then produce the optical path difference shown in Fig. 1. In the main section of the grating, monochromatic light at a wavelength of λ is incident on the grating surface to be measured, where the angle of incidence on the grating is denoted by α and the diffraction angle of the grating

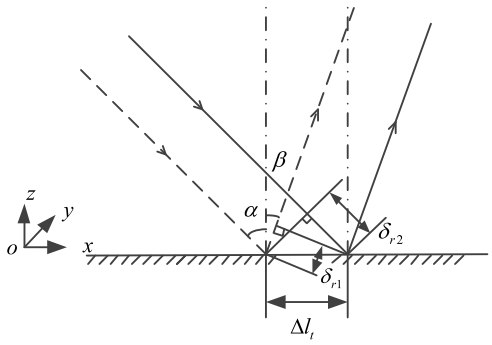

Fig. 1. Schematic of optical path difference due to the changes in the refractive index of air.

is denoted by β. The grating groove direction is in the y direction (which lies perpendicular to the plane of the paper), and the optical path difference produced by the groove position error can be given as

$$\delta_r = \delta_{r1} + \delta_{r2} = \Delta l_t \cdot (\sin\alpha + \sin\beta) \tag{4}$$

The grating diffraction equation is given as follows:

$$d \cdot (\sin\alpha + \sin\beta_m) = m \cdot \lambda \tag{5}$$

where d is the grating constant, β_m is the mth-order diffraction angle, m is the grating diffraction order and λ is the incident light wavelength.

By combining Eqs. (3)–(5), the diffraction wavefront error of the grating can then be written as

$$\Delta(m) = (n_t - n_c) \cdot l_t \cdot (\cos\alpha + \cos\beta_m) \tag{6}$$

3. Measurement of the changes in the refractive index of air

3.1. Indirect measurement method

The indirect measurement method is used to obtain the changes in the refractive index of air from the empirical equation and the measured values of the temperature, pressure and humidity. In this paper, we use the latest version of the Edlen equation to calculate the refractive index of air [22–25].

The improved dispersion formula for standard air at 1 atm, 20 °C, and 0.04% carbon dioxide content was given as:

$$(n-1)_s \cdot 10^8 = 8091.37 + \frac{2333983}{130 - \sigma^2} + \frac{15518}{38.9 - \sigma^2} \tag{7}$$

where σ is the vacuum wavenumber in μm^{-1}.

The following expression was used to determine the refractivity of air when containing x parts by volume of carbon dioxide:

$$(n-1)_x = [1 + 0.5327 \cdot (x - 0.04\%)] \cdot (n-1)_s \tag{8}$$

The refractivity of standard dry air at temperature T and atmospheric pressure p is given as:

$$(n-1)_{tp} = \frac{(n-1)_x \cdot p}{93214.60} \cdot \frac{1 + 10^{-8} \cdot (0.5953 - 0.009876 \cdot T) \cdot p}{1 + 0.0036610 \cdot T} \tag{9}$$

To determine the difference between the refractive index of moist air containing a partial pressure f of water vapor and that of dry air at the same total pressure, the following revised expression was obtained:

$$n_{tpf} - n_{tp} = -f \cdot (3.8020 - 0.0384 \cdot \sigma^2) \cdot 10^{-10} \tag{10}$$

The pressure f of the water vapor is the partial pressure generated by the water content in the air. The humidity sensor that we used in the experiments measures the relative humidity h in the air rather than the water vapor pressure f. The relative humidity h is the ratio of the

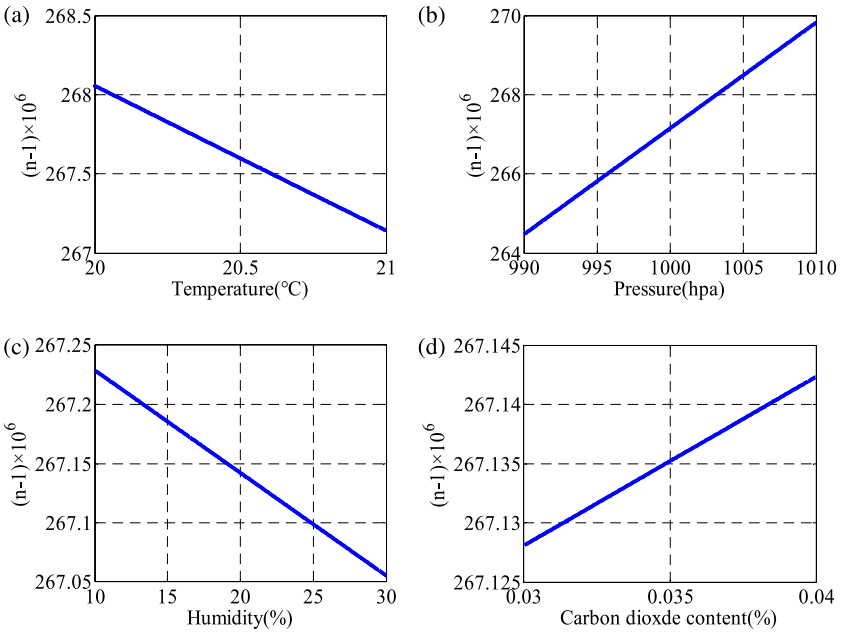

Fig. 2. Effects of air temperature, pressure and humidity on the refractive index. (a) Temperature; (b) pressure; (c) humidity; and (d) carbon dioxide content.

water vapor pressure f to the saturated vapor pressure F at the same temperature and it can be expressed as:

$$h = \frac{f}{F} \times 100\% \tag{11}$$

Eqs. (7)–(11) can be combined to allow the refractive index of air to be written as:

$$\begin{aligned}(n-1)_{tpf} = {} & \frac{10^{-8} \cdot [1 + 0.5327 \cdot (x - 0.04\%)] \cdot p}{93214.60} \\ & \cdot (8091.37 + \frac{2333983}{130 - \sigma^2} + \frac{15518}{38.9 - \sigma^2}) \cdot \\ & \frac{1 + 10^{-8} \cdot (0.5953 - 0.009876 \cdot T) \cdot p}{1 + 0.0036610 \cdot T} \\ & - h \cdot F \cdot (3.8020 - 0.0384 \cdot \sigma^2) \cdot 10^{-10}\end{aligned} \tag{12}$$

The operating wavelength λ of the dual-frequency laser is 632.8 nm, and the wavenumber σ, which is the reciprocal of the wavelength, is (1/0.6328) μm^{-1}; the saturated vapor pressure F at 20 °C is 2338.43 Pa. Based on Eq. (12), we studied the effects of the temperature, pressure, humidity and carbon dioxide content of the air on the refractive index, and the results are presented in Fig. 2. Fig. 2(a) shows the effect of the air temperature on the refractive index when p is 1 atm, x is 0.04%, and h is 20%; Fig. 2(b) shows the effects of the pressure on the refractive index when T is 20 °C, x is 0.04%, and h is 20%; Fig. 2(c) shows the effects of the humidity on the refractive index when T is 20 °C, p is 1 atm and x is 0.04%; Fig. 2(d) shows the effects of the carbon dioxide content on the refractive index when T is 20 °C, p is 1 atm, and h is 20%. For ease of analysis, we make the following two assumptions: (1) the changes in temperature, pressure, humidity and CO_2 content are uniform; and (2) the dead path length is 36 mm. The refractive index change values shown in Fig. 2 were inserted into Eq. (6) to calculate the diffraction wavefront error of an echelle grating with a dimension perpendicular to the grooves of 500 mm, a blazed order of −36 and a groove density of 79 grooves/mm; the calculation results are listed in Table 1.

As shown by the results in Fig. 2 and Table 1, if uncompensated, the wavefront error of the echelle grating will vary by 0.0873λ per °C, 0.511λ per 20 hPa pressure change, 0.0166λ per 20% change in relative humidity, and 0.0014λ ppm per 0.01% change in carbon dioxide content. To obtain a high-quality ruled grating, we must compensate for the groove errors caused by the changes in the refractive index of air.

The temperature, in addition to affecting the changes in the refractive index of the air, also affects the deformation of the ruling engine components, which thus also affects the grating groove errors. Therefore, strict temperature control is required when ruling gratings and the temperature fluctuation of the core ruling area is expected to be better than ±0.01 °C.

In recent decades, the rapid increase in the population and rapid industrial development means that the carbon dioxide produced by breathing and by the combustion of coal, oil and natural gas has caused the carbon dioxide content of the atmosphere to increase. However, the carbon dioxide content takes tens of years or more to change by 0.01%, and we thus believe that the carbon dioxide content does not change during 10 days of grating ruling experiments. Even if the carbon dioxide content did change by 0.01%, the results in Table 1 show that the effect on the grating wavefront is very small. Therefore, we do not consider the effect of the carbon dioxide content on the grating wavefront in this paper.

The indirect measurement method is mainly based on the empirical formula, and the disadvantage of this approach is that while the method can compensate for variations in the air temperature, pressure, and humidity, it fails to detect index changes caused by excess CO_2, oil vapors, the operator, and other sources.

3.2. Direct measurement method

In contrast to the indirect measurement method, which requires an empirical formula, a method that uses a wavelength tracker to obtain the changes in the refractive index is called the direct measurement method. The wavelength tracker shown in Fig. 3 uses a differential interferometer to measure changes in the distance between the mirrors at the two ends of a Zerodur bar. Because Zerodur has an ultra-low coefficient of thermal expansion and the temperature of the core ruling area is strictly controlled, the measured dimensional changes are caused entirely by the changes in the refractive index.

From Eqs. (1)–(3), the values of the change in refractive index Δn_t acquired by the direct measurement method can be written as

$$\Delta n_t = -\frac{n_0^2 \cdot \Delta d_t}{n_c \cdot d_c + n_0 \cdot \Delta d_t} \tag{13}$$

where n_0 is the initial refractive index value, Δd_t is the change in the distance between mirrors at the two ends of the Zerodur bar, and d_c is the calibrated length of the Zerodur bar.

Table 1
Effects of the refractive index change values shown in Fig. 2 on the diffraction wavefront error of an echelle grating with dimensions of 400 mm × 500 mm, a blazed order of −36 and a groove density of 79 grooves/mm.

Parameter	T	p	h	CO_2
Variation range	20 ~ 21°C	990 ~ 1010 hpa	10 ~ 30%	0.03 ~ 0.04%
The peak to valley (PV) value of Δn	9.1361×10^{-7}	5.343×10^{-6}	1.7316×10^{-7}	1.422×10^{-8}
The peak to valley (PV) value of $\Delta(m)$	0.0873λ	0.511λ	0.0166λ	0.0014λ

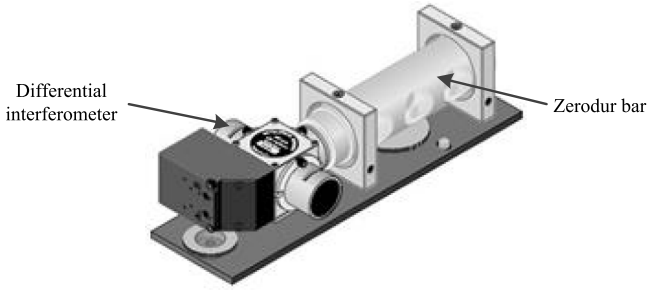

Fig. 3. Wavelength tracker.

However, the disadvantage of this method is that the wavelength tracker can only obtain changes in the refractive index relative to its initial value and cannot give the absolute refractive index value.

3.3. The method that was used in the CIOMP-6 ruling engine

The CIOMP-6 ruling engine takes full advantage of both of the above methods to achieve real-time compensation for groove errors caused by the refractive index of air. Specifically, the indirect measurement method is used to obtain the initial refractive index value n_0 from Eq. (12) and the direct measurement method is used to measure the value of the change Δd_t in the distance between mirrors at the two ends of the Zerodur bar at any time t, which means that the refractive index n_t at any time t is then given by

$$n_t = n_0 + \Delta n_t \tag{14}$$

From Eqs. (3) and (14), to eliminate the effect of the refractive index change on the gratings, the correction for the groove position errors can be calculated as:

$$\Delta l_t = (n_0 + \Delta n_t - n_c) \cdot l_t \tag{15}$$

By taking Eq. (15) into Eq. (6), the diffraction wavefront of the grating can then be expressed as:

$$\Delta(m) = (n_0 + \Delta n_t - n_c) \cdot l_t \cdot (\cos\alpha + \cos\beta_m) \tag{16}$$

4. Ruling results

4.1. Before the correction of the groove errors caused by the refractive index of air

Before the environment of the CIOMP-6 ruling engine was strictly controlled and the groove errors caused by changes in the refractive index of air were compensated, we ruled a 75 mm × 150 mm echelle grating with a groove density of 79 grooves/mm and monitored the variation in the environment during grating ruling with temperature, pressure, and humidity sensors and the wavelength tracker. As shown in Fig. 4, the pressure change trend is consistent with the trend observed in the measured data using the wavelength tracker, which indicates that pressure plays a major role in the refractive index change under current environmental change conditions.

By combining the data given in Fig. 4 with Eqs. (12)–(14), we can use the indirect measurement method and the method that was used in the CIOMP-6 ruling engine to obtain the refractive index values as shown in Fig. 5. Fig. 5 shows that the refractive index changes obtained using the two methods are consistent and also confirms that the trend in the curves shown in Fig. 5 is similar to the trend shown in the

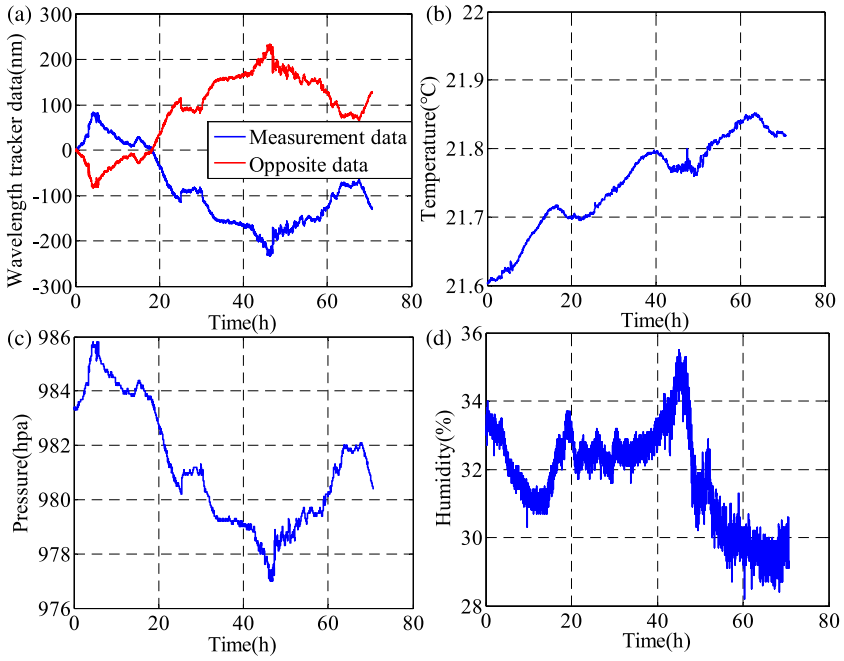

Fig. 4. Variation of the ruling environment during ruling of the 75 mm × 150 mm echelle grating. (a) Wavelength tracker data; (b) temperature; (c) pressure; and (d) humidity data.

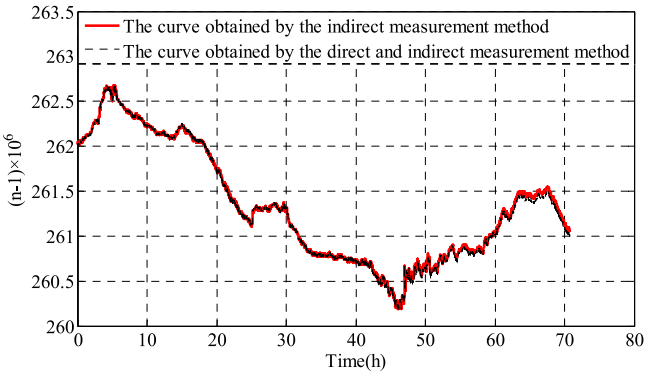

Fig. 5. Effect of changes in the refractive index of air on the diffraction wavefront during ruling of the 75 mm × 150 mm echelle grating.

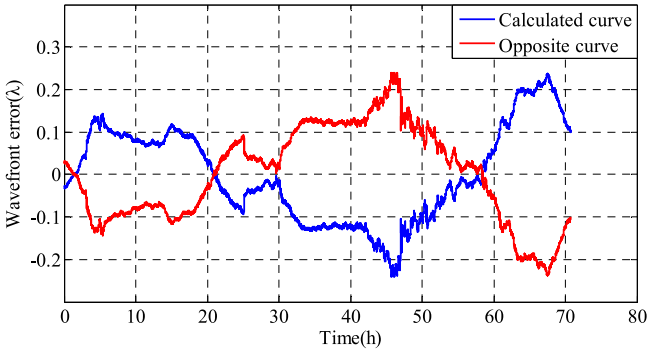

Fig. 6. Calculated curves of the wavefront of the 75 mm × 150 mm echelle grating at the diffraction order caused by the refractive index of air.

measurement data from the wavelength tracker and the trend of the pressure curve in Fig. 4.

We take the data for the refractive index of the air obtained via the direct and indirect measurement methods, as shown in Fig. 5, into Eq. (16) and obtain the curve and the opposite curve for the

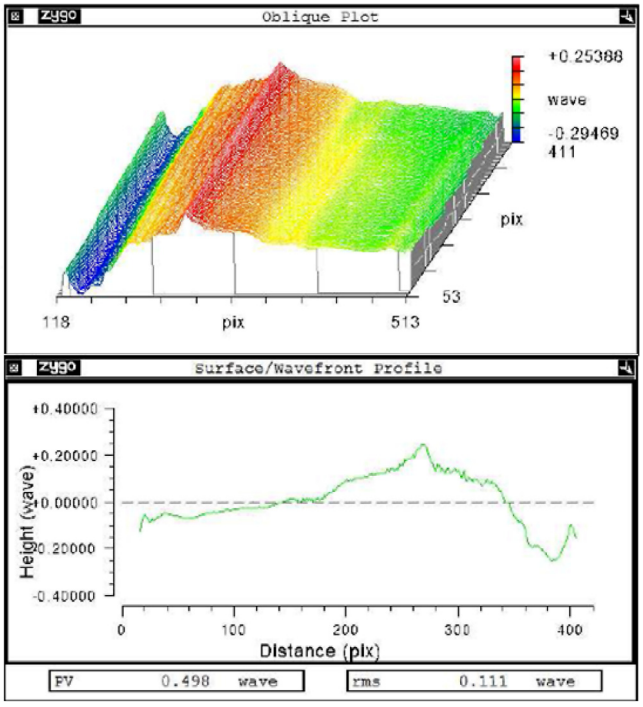

Fig. 7. Wavefront error of the 75 mm × 150 mm echelle grating at the diffraction order.

wavefront of the 75 mm × 150 mm echelle grating diffraction order (−36th), as illustrated in Fig. 6. Fig. 6 shows the calculated PV value of wavefront of the ruled grating at the diffraction order is 0.4773λ (where λ = 632.8 nm). As shown in Fig. 7, the measured PV value of the grating wavefront profile at 632.8 nm for a blazed order of −36 is 0.498λ . Comparison of Fig. 6 with Fig. 7 shows that the calculated PV value and the opposite curve of the echelle grating wavefront obtained from the measured data and the measured PV value and the surface/wavefront profile curves of the echelle grating

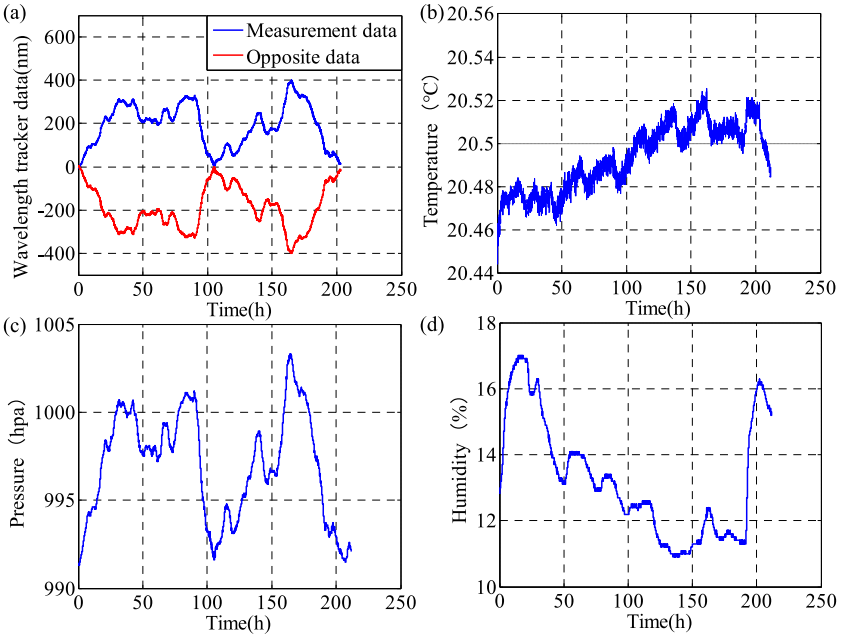

Fig. 8. Variation in the ruling environment during ruling of the 300 mm × 470 mm echelle grating. (a) Wavelength tracker data; (b) temperature; (c) pressure; and (d) humidity data.

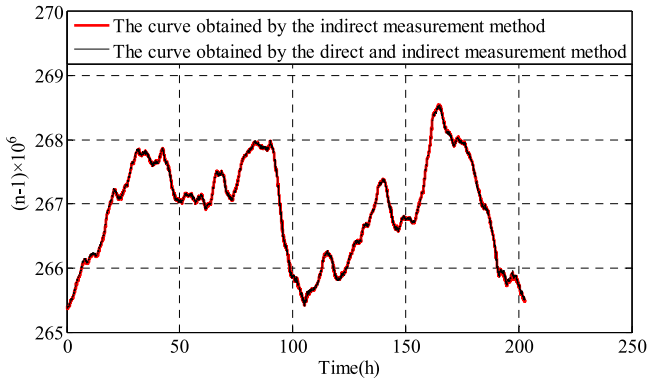

Fig. 9. Effect of changes in the refractive index of air on the diffraction wavefront during ruling of the 300 mm × 470 mm echelle grating.

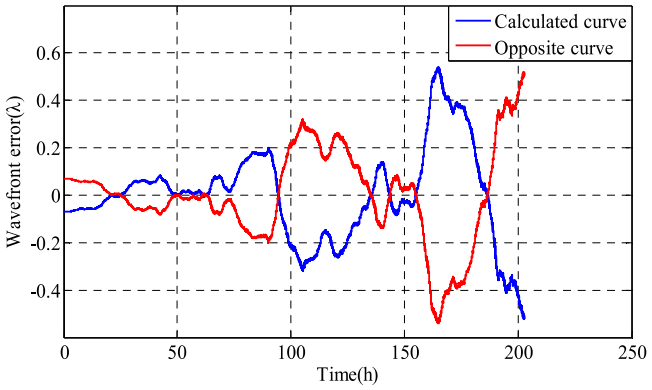

Fig. 10. Calculated curves of the wavefront of the 300 mm × 470 mm echelle grating at the diffraction order caused by the refractive index of air.

are similar, respectively, thus indicating that the grating wavefront is mainly affected by changes in the refractive index.

4.2. After the correction of the groove errors caused by the refractive index of air

After the temperature of the room in which the ruling engine is located is strictly controlled, the groove errors caused by the refractive index changes were compensated in real time, and we ruled a 300 mm × 470 mm echelle grating with a groove density of 79 grooves/mm. The data that were measured using the wavelength tracker and the temperature, humidity, and pressure sensors during grating ruling are shown in Fig. 8. Fig. 8(a) and (c) show that the consistency of the pressure trend and the wavelength tracker data indicate that the refractive index change is mainly affected by the air pressure. Fig. 8(b) shows that the fluctuation in the core ruling area is better than ±0.04 °C.

We take the data from Fig. 8 into Eqs. (12)–(14) to obtain the refractive index curves shown in Fig. 9, where the red solid line and the black dashed line represent the refractive index measured by the direct measurement method and that measured by the method we used in the CIOMP-6 ruling engine, respectively. The results in Fig. 9 show that the refractive index data obtained by these two methods is perfectly matched. Comparison of Figs. 8 and 9 shows that the trend of the refractive index change is consistent with the trends in the pressure and the wavelength tracker, thus indicating that the refractive index is mainly affected by the air pressure during grating ruling.

By combining the air refractive index data obtained by the direct and indirect measurement methods with Eq. (16), we obtain the curve and the opposite curve of the wavefront of the 300 mm × 470 mm echelle grating at the diffraction order (−35th), as shown in Fig. 10.

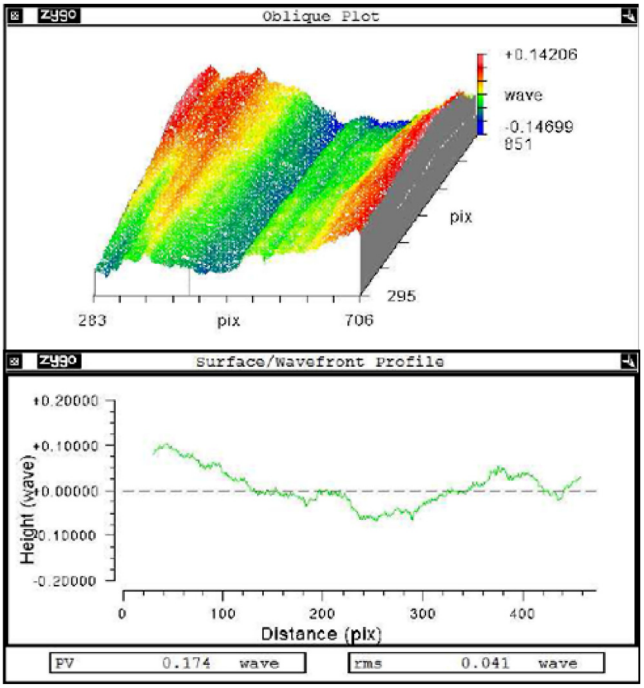

Fig. 11. Wavefront error of the 300 mm × 470 mm echelle grating at the diffraction order.

Fig. 10 shows that the calculated PV value of ruled grating wavefront at the diffraction order is 1.0618λ (where λ = 632.8 nm). Fig. 11 shows that the measured PV value of the wavefront profile of the grating at 632.8 nm at a blazed order of −35 is 0.174λ. Comparison of Figs. 10 and 11 shows that the refractive index profile obtained from the measured data and the surface/wavefront profile curve of the grating are not similar, while the PV value of the wavefront profile is significantly reduced after compensation of the groove errors caused by the refractive index.

5. Conclusions

To reduce the effects of groove errors caused by the refractive index of air on the wavefront of a ruled grating, we studied the relationship between the refractive index of air and the grating wavefront systematically. We have established a mathematical model of the relationship between the refractive index of air and the grating wavefront. We then introduced two methods to measure the refractive index of the air, used the Edlen equation to analyze the effects of temperature, pressure and humidity on the grating wavefront, and used the advantages of the two measurement methods to obtain the compensation value for the groove error. Before and after compensation of the groove errors caused by the refractive index change, we separately ruled two echelle gratings. Comparison of the wavefront values based on the refractive index data with the measured wavefront values of the gratings indicate that compensation of the groove errors caused by the refractive index change significantly improves the grating diffraction wavefronts.

Acknowledgments

The authors gratefully acknowledge supports for this work from the Chinese Ministry of National Science and Technology Program (2016YFF0102006, 2016YFF0103304), the National Natural Science Foundation of China (NSFC) (61605204) and the Natural Science Foundation of Jilin Province, China (20190201104JC).

References

[1] T. Sakanoi, Y. Kasaba, M. Kagitani, H. Nakagawa, J. Kuhn, S. Okana, Development of infrared echelle spectrograph and mid-infrared heterodyne spectrometer on a small telescope at Haleakala, Hawaii for planetary observation, in: Proc. SPIE, Vol. 9147, 2014, 91478D.

[2] X. Mi, S. Zhang, X. Qi, H. Yu, H. Yu, Y. Tang, Ruling engine using adjustable diamond and interferometric control for high-quality gratings and large echelles, Opt. Express 27 (14) (2019) 19448–19462.

[3] B. Zhang, Z. Wang, S. Brodbeck, C. Schneider, M. Kamp, S. Höfling, H. Geng, Zero-dimensional polariton laser in a subwavelengh grating-based vertical microcavity, Light Sci. Appl. 3 (2014) 1–5.

[4] F. Cheng, J. Zhang, D. Wang, Z. Gu, N. Zhuo, S. Zhai, L. Wang, J. Liu, S. Liu, Z. Wang, Demonstration of high-power and stable sing-mode in a quantum Cascade laser using buried sampled grating, Nanoscale Res. Lett. 14 (2019) 123.

[5] T. Lei, M. Zhang, Y. Li, P. Jia, G. Ning Liu, X. Xu, Z. Li, C. Min, J. Lin, C. Yu, H. Niu, X. Yuan, Massive individual orbital angular momentum channels for multiplexing enabled by Dammann gratings, Light Sci. Appl. 4 (2015) 1–7.

[6] H. Xu, Y. Shi, Subwavelength-grating-assited silicon polarization rotator covering all optical communication bands, Opt. Express 27 (4) (2019) 5588–5597.

[7] J. Qiao, A.W. Schmid, L.J. Waxer, T. Nguyen, J. Bunkenburg, C. Kingsley, A. Kozlov, D. Weinerl, In situ detection and analysis of laser-induced damage on a 1.5-m multilayer-dielectric grating compressor for high-energy, petawatt-class laser systems, Opt. Express 18 (10) (2010) 10423–10431.

[8] A. Cotel, M. Castaing, P. Pichon, C. Le Blanc, P hased-array grating compression for high-energy chirped pulse amplification lasers, Opt. Express 15 (5) (2007) 2742–2752.

[9] 2019. https://lasers.llnl.gov/science/photo-science/advanced-optics.

[10] T. Jitsuno, S. Motokoshi, T. Okamoto, D. Smith, M.L. Schattenburg, H. Kitamura, H. Matsuo, T. Kawasaki, K. Kondo, H. Shirage, Y. Nakata, H. Habara, K. Tsubakimoto, R. Kodama, K.A. Tanaka, N. Miyanaga, K. Mima, Development of 91 cm size gratings and mirrors for LEFX laser system, J. Phys. Conf. Ser. 112 (3) (2008) 032002.

[11] X. Mi, S. Zhang, X. Qi, H. Yu, J. Zhou, S. Jiang, Effect of thickness non-uniformity of large-area grating metal film on grating diffraction wavefront, Opt. Laser Technol. 119 (2019) 105675.

[12] X. Mi, H. Yu, H. Yu, S. Zhang, X. Li, X. Yao, X. Qi, Bayinheshig, Q. Wang, Correcting groove error in gratings ruled on a 500-mm ruling engine using interferometric control, Appl. Opt. 56 (21) (2017) 5857–5864.

[13] G.R. Harrison, The production of diffraction gratings I. Development of the ruling art, J. Opt. Soc. Am. 39 (6) (1949) 413–426.

[14] D.A. Dzvies, G.M. Stiff, Diffraction grating ruling in Australia, Appl. Opt. 8 (7) (1969) 1379–1384.

[15] X. Mi, S. Zhang, H. Yu, H.i Yu, M. Cong, X. Qi, Using a unique mirror to minimize the effect of ruling engine cosine error on grating performance, Appl. Opt. 57 (35) (2018) 10146–10151.

[16] W.R. Horsfield, Ruling engine with hydraulic drive, Appl. Opt. 4 (2) (1965) 189–193.

[17] C. Mitchell, Diffraction grating fabrication in Australia, Spectrochim. Acta At. Spectrosc. 54 (14) (1999) 2041–2049.

[18] M.C. Hutley, Diffraction Gratings, first ed., Academic press, London, 1982, Chap.1.

[19] G.R. Harrison, S.W. Thompson, H. Kazukonis, J.R. Connell, 750-mm ruling engine producing large gratings and echelles, J. Opt. Soc. Am. 62 (6) (1972) 751–756.

[20] T. Kita, T. Harada, Ruling engine using a piezoelectric device for large and high-groove density gratings, Appl. Opt. 31 (10) (1992) 1399–1406.

[21] C. Yang, X. Li, H. Yu, H. Yu, J. Zhu, S. Zhang, J. Gao, Bayanheshig, Y. Tang, Practical method study on correcting yaw error of 500mm grating blank carriage in real time, Appl. Opt. 54 (13) (2017) 4084–4088.

[22] Bengt Edlen, The refractive index of air, Metrologia 2 (2) (1966) 71–80, (1966).

[23] K.P. Birch, M.J. Downs, The results of a comparison between calculated and measured values of the refractive index of air, J. Phys. E: Sci. Instrum. 21 (1988) 694–695.

[24] K.P. Birch, M.J. Downs, An updated Edlen equation for the refractive index of air, metrologia 30 (1993) 155–162.

[25] K.P. Birch, M.J. Downs, Correction to the updated Edlh equation for the refractive index of air, metrologia 31 (1994) 315–316.